

Time-Optimal Path Planning in Dynamic Flows using Level Set Equations: Realistic Applications.

T. Lolla · P. J. Haley Jr. · P. F. J. Lermusiaux

Received: date / Accepted: date

Abstract The level set methodology for time-optimal path planning is employed to predict collision-free and fastest time trajectories for swarms of underwater vehicles deployed in the Philippine Archipelago region. To simulate the multiscale ocean flows in this complex region, a data-assimilative primitive-equation ocean modeling system is employed with telescoping domains that are interconnected by implicit two-way nesting. These data-driven multiresolution simulations provide a realistic flow environment, including variable large-scale currents, strong jets, eddies, wind-driven currents and tides. The properties and capabilities of the rigorous level set methodology are illustrated and assessed quantitatively for several vehicle types and mission scenarios. Feasibility studies of all-to-all broadcast missions, leading to minimal time transmission between source and receiver locations, are performed using a large number of vehicles. The results with gliders and faster propelled vehicles are compared. Reachability studies, i.e. determining the boundaries of regions that can be reached by vehicles for exploratory missions, are then exemplified and analyzed. Finally, the methodology is used to

determine the optimal strategies for fastest time pick-up of deployed gliders by means of underway surface vessels or stationary platforms. The results highlight the complex effects of multiscale flows on the optimal paths, the need to utilize the ocean environment for more efficient autonomous missions and the benefits of including ocean forecasts in the planning of time-optimal paths.

Keywords path planning · level set · reachability · dynamic flows · multiscale · ocean sampling · AUVs · gliders · swarms · time-optimal · energy-optimal · MSEAS

1 Introduction.

In Part-1 of this two part paper (Lolla et al, 2014), we described a rigorous methodology for time-optimal path planning of autonomous vehicles navigating in strong and dynamic currents. The methodology utilizes level set methods to solve a Hamilton-Jacobi equation that exactly governs the evolution of the reachability front. The optimal trajectory is then determined by solving a particle tracking ordinary differential equation backward in time. For convenience, we have included a brief description of the methodology, the algorithm, and the relevant notation in §A. A review of the relevant literature was previously provided in Lolla et al (2014).

In the present manuscript, we illustrate and analyze the capabilities of our methodology in the multiscale flows of the Philippine Archipelago, for a wide range of planning scenarios and vehicle types. The Philippine Archipelago is chosen because of its complex geometry, with numerous islands, passages and semi-enclosed seas, and its multiscale dynamics arising due to the

T. Lolla
Department of Mechanical Engineering, Massachusetts Institute of Technology, 77 Mass. Ave., Cambridge, MA - 02139
Tel.: 617-253-7799
E-mail: ltapovan@mit.edu

P. J. Haley Jr.
Department of Mechanical Engineering, Massachusetts Institute of Technology, 77 Mass. Ave., Cambridge, MA - 02139
Tel.: 617-253-6824
E-mail: phaley@mit.edu

P. F. J. Lermusiaux
Department of Mechanical Engineering, Massachusetts Institute of Technology, 77 Mass. Ave., Cambridge, MA - 02139
Tel.: 617-324-5172
E-mail: pierrel@mit.edu

1
2
3
4
5
6
7
8
9
10
11
12
13
14
15
16
17
18
19
20

large-scale open ocean and atmospheric forcing, energetic mesoscale currents and eddies, and strong tides and internal waves both in narrow straits and at steep shelf breaks. Such conditions provide challenging environments for the planning of autonomous underwater missions.

In what follows, §2 outlines the ocean modeling system employed for the region and the corresponding multiscale ocean flows and their evolution, highlighting key characteristics for the autonomous vehicles. In §3.1, we compute, compare and analyze the time-optimal paths of 1600 gliders and propelled vehicles performing all-to-all broadcast missions through the Archipelago. The effects of the multiscale flows and vehicle speeds on the trajectories and on the overall information transmission rates are discussed and synthesized. In §3.2, we consider the deployment of vehicles and complete reachability analyses for the Sulu Sea, i.e. we predict the portions of the Sulu Sea that can be reached and explored within a certain time for a set of deployment locations. In §3.3, we consider the recovery of vehicles and fastest interception with other platforms. Specifically, we predict the trajectories for autonomous vehicles that lead to the fastest time pick-up by either underway or fixed platforms. Conclusions are provided in §4.

2 Multiresolution Ocean Modeling System and Multiscale Ocean Flow Field

Multiresolution Ocean Modeling and Data-assimilative Simulations. To predict the multiscale ocean flow dynamics in the Philippine Archipelago region, we employ the MIT Multidisciplinary Simulation, Estimation, and Assimilation System (MSEAS) (Haley and Lermusiaux, 2010; MSEAS Group, 2010). The MSEAS software is used for fundamental research and for realistic tidal-to-mesoscale simulations and predictions in varied regions of the world’s ocean (Leslie et al, 2008; Onken et al, 2008; Haley et al, 2009; Gangopadhyay et al, 2011; Ramp et al, 2011; Colin et al, 2013), including monitoring (Lermusiaux et al, 2007), real-time ecosystem and acoustic predictions (Beşiktepe et al, 2003; Xu et al, 2008) and environmental management (Cossarini et al, 2009).

The present ocean field estimates are from data-assimilative simulations for the Philippine Archipelago region during February 5 – March 24, 2009, as part of the Philippine Straits Dynamics Experiment (PhilEx; Gordon and Villanoy, 2011). The multiresolution simulations (Lermusiaux et al, 2011) solve the hydrostatic primitive-equations with a nonlinear free surface, using second-order structured finite volumes and a set of telescoping domains interconnected by implicit two-way

nesting (Haley and Lermusiaux, 2010). The domains have 9 km, 3 km and 1 km horizontal resolutions and 70 optimized vertical levels. The simulations are initialized using the February NODC World Ocean Atlas 2005 (WOA05) climatology mapped with the Fast-Marching-Method-based Objective Analysis (Agarwal and Lermusiaux, 2011). The corresponding velocities are obtained solving an optimization problem (Haley et al, 2014), combining: geostrophic balance; velocity anomalies derived from Sea Surface Height (SSH) anomaly, itself obtained from the Colorado Center for Astrodynamic Research (CCAR; Leben et al, 2002); feature model velocities for the South China Sea and the bottom currents through the Mindoro and Dipolog Straits; and, open boundary transports from the HYbrid Coordinate Ocean Model (HYCOM; Bleck, 2002; Hurlburt et al, 2011). The simulations were forced with atmospheric fluxes from the Coupled Ocean/Atmosphere Mesoscale Prediction System (COAMPS; Hodur, 1997) and barotropic tides created using Logutov and Lermusiaux (2008) with boundary forcing from OTIS (Egbert and Erofeeva, 2002). Additional information on these simulations are provided in (Lermusiaux et al, 2011).

Multiscale Ocean Flow Field Encountered by Vehicles. The new Hamilton-Jacobi level set equation (6) (§A) for autonomous time-optimal path planning contains a term for the advection by ocean currents. Hence, an estimate of the evolution of these currents at the location of the dynamic zero level set is needed. The currents are here obtained from our MSEAS multiresolution simulations. For the present applications, we assume that all vehicles follow the same yo-yo pattern in the vertical and that the ocean vertical velocities (which are relatively small) do not have much effect on the forward motions of vehicles. The yo-yo pattern is chosen because it is commonly utilized by gliders or propelled vehicles collecting in situ data for ocean exploration. The utilization of the same behavior in the vertical for all vehicles also allows a direct comparison across vehicles, regardless of the vehicle type. With these assumptions, what differentiates the vehicles is then simply their nominal forward horizontal speeds in these yo-yo vertical-horizontal motions. And what facilitates (or impedes) this forward motion are then the horizontal currents that the vehicles encounter during their yo-yo motions.

For the Archipelago region, to sample the thermocline, we consider yo-yo patterns from the near surface to either the local near bottom or 400 m depth, whichever is shallower. We assume that the time scales of the horizontal currents variability are not much shorter than the time to complete a single vertical excursion. Within our assumptions, the horizontal currents that a

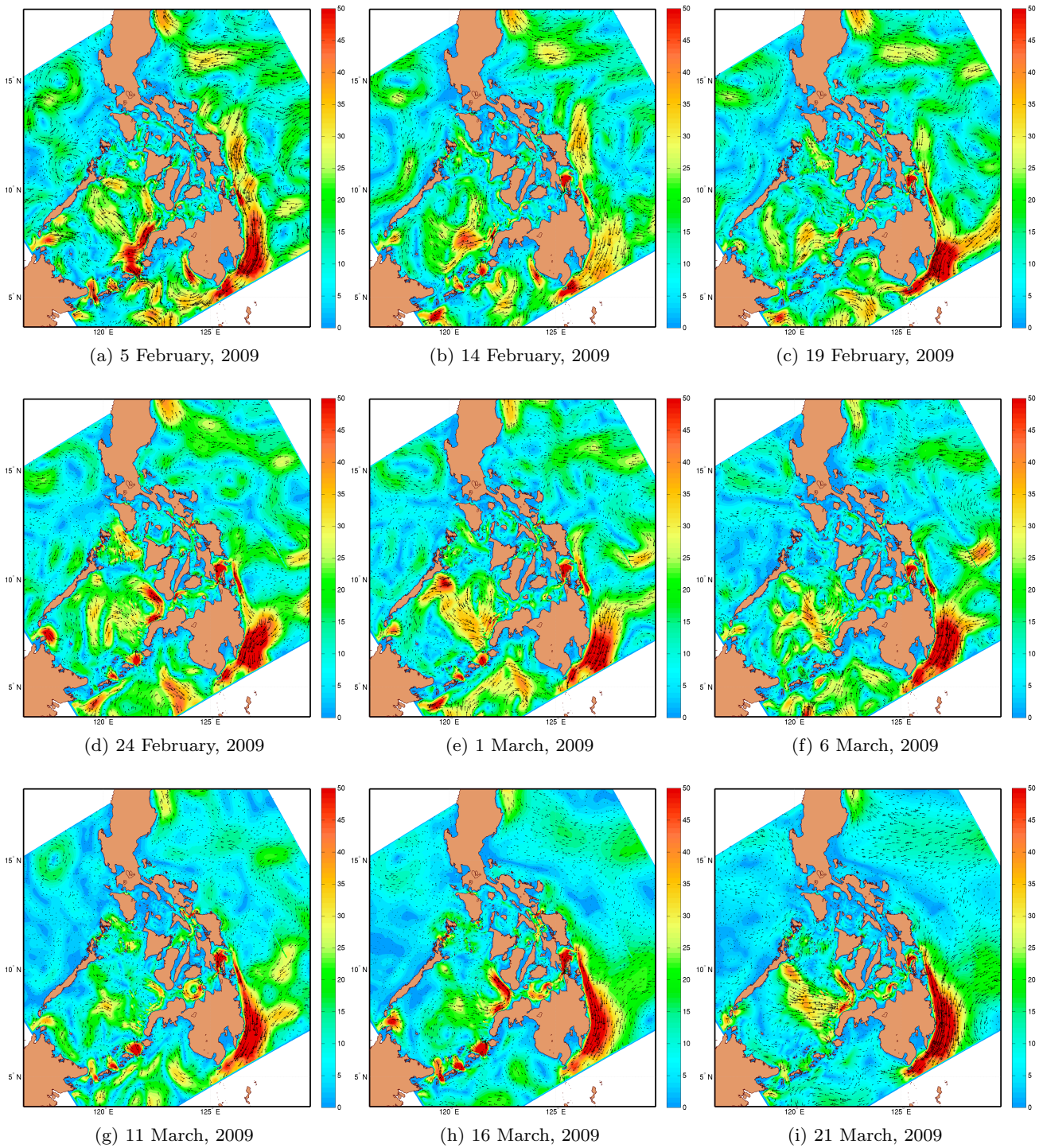


Fig. 1: Snapshots of the vertically-averaged horizontal ocean flow-field in the Philippine Archipelago on different days of the Philippine Straits Dynamics Experiment (day 1, day 10 and then every 5 days). Horizontal currents shown are those encountered by vehicles in a yo-yo pattern from the near surface to either the local near bottom or 400 m depth, whichever is shallower. Flow patterns are illustrated by their streamlines, overlaid on a color plot of the flow magnitude (in cm/s).

125 vehicle would actually encounter during its yo-yo motion
 126 would be the horizontal currents integrated along
 127 its path, from the near surface to either the local near

bottom or 400 m depth. Hence, in what follows, we
 illustrate and discuss these vertically-averaged horizontal
 currents. They are the horizontal currents that force

128

129

130

our simulated vehicles, for all nominal vehicle speeds and specific paths we consider. They are illustrated in Fig. 1. Of course, it is the path of the vehicle that determines which currents are actually encountered, hence the need for time-optimal path planning.

In the Pacific Ocean, the large-scale horizontal flow encountered by the vehicles (Fig. 1) consists of the North Equatorial Current (NEC) and its active eddy field formed as the NEC impinges upon the Archipelago around 14°N (Qu and Lukas, 2003) and then splits into two boundary currents, the equatorward Mindanao current and the northward Kuroshio. A portion of the Mindanao current flows along the island of Mindanao into the eastern and northern Sulawesi Sea. There, exchanges occur with the Sulu Sea through the many straits of the Sulu Archipelago and its strong tides and pulsating strait flows. The exchanges between the Pacific and the Sulu Sea also occur through the Luzon Strait (outside of the modeling domain) via the South China Sea and the Balabac and Mindoro straits, through the San Bernardino Strait and the Sibuyan Sea, and through the Surigao Strait and the Bohol Sea and Dipolog Strait. These flows are variable and observed in both directions, either in or out of the Sulu Sea (Fig. 1).

Restricting our attention to the 0-400 m mean flows encountered by the vehicles, in the Mindoro Strait system, they are mostly southward into the Sulu Sea (Lermusiaux et al, 2011) but, as shown on Fig. 1, these flows are highly variable on multiple scales in response to Monsoon winds, mesoscale dynamics and tides. Although tidally very active, the mean flows through the San Bernardino strait are small (Gordon et al, 2011). The neighbouring current systems in the Sibuyan Sea are also variable but relatively weak, and thus will have smaller effects on vehicles entering or leaving the Sulu Sea. Tidal currents are also very strong at the Surigao Strait, but on average, the upper currents show mostly an inflow from the Pacific through Surigao Strait into the Bohol Sea. These currents join up with eddies in the Bohol Sea and with the Bohol jet meandering mostly along the northern edge of the Bohol Sea. The 0-400 m flows then continue through Dipolog Strait and into the Sulu Sea (see also Gordon et al, 2011; Hurlburt et al, 2011). Once in the Sulu Sea, most of the time, vehicles will encounter a relatively strong cyclonic eddy and northward current along Negros Island. However, there are time periods when that current reverses, for example, for a week or so around 14 February, 2009 (Fig. 1b).

The Sulu Sea in the 0-400 m depth range has a complex and intermittent eddy field. On monthly average, the Sulu Sea has net inflows from Balabac, Mindoro/Panay and Dipolog straits, and net outflows through the Sibutu Passage and the Sulu Archipelago. Although

the latter are net outflows on average, they are tidally very active with internal tides and waves, and they experience strong episodic net inflows from the Sulawesi Sea. The Sulawesi is also relatively very active with variable meandering jets, intermittent mesoscale eddies and coastal currents. In the South China Sea just north of Palawan island, the currents are also variable but often weaker than those in the Sulawesi Sea.

3 Applications in Complex Multiscale Ocean Conditions.

In this section, we evaluate the performance and illustrate the capabilities of our methodology (Lolla et al, 2014) by applications to autonomous missions in realistic conditions. Path-planning in the Philippines domain (Fig. 1) is challenging due to the complex geometry with many islands and the strong and dynamic multiscale ocean currents and tides. Some of the questions that motivate the missions that we consider are: Can our new rigorous methodology be applied to such realistic but complex dynamics and multiply-connected domains? How do the time-optimal paths look for large numbers of vehicles operating in different regions? How do these paths and the corresponding reachability sets relate to the flow features? How sensitive are the paths to the speed of the vehicles and to the locations of their start and end points? And finally, what is the computational cost of our algorithm and can our implementation be utilized in real-time, even for situations with many more vehicles that are typically employed today?

For the computations of the optimal level set ϕ^o and backward trajectories \mathbf{X}_P^* , all results presented next solve (6) and (8) using the numerical schemes obtained in Lolla et al (2014) and summarized here in §A.2. For ϕ^o , a spatial discretization of $3\text{ km} \times 3\text{ km}$ resolution and a time-step of 5 min (chosen according to the Courant-Freidrichs-Lewy (CFL) criterion) are employed. Grid points that lie inside the islands are masked in all computations involved in solving (6). Open boundary conditions are enforced on all domain boundaries. For the numerical integration, space and time are non-dimensionalized by reference values of $L_{\text{ref}} = 3\text{ km}$ and $T_{\text{ref}} = 3\text{ hr}$, respectively. As a result, velocities are non-dimensionalized by $U_{\text{ref}} = \frac{L_{\text{ref}}}{T_{\text{ref}}} = 1\text{ km/hr}$.

3.1 All-to-all Broadcasts Through The Archipelago.

Analyses of various scenarios of all-to-all broadcast missions through the Archipelago are now performed for several vehicle types. All-to-all broadcast is a term generally used in parallel distributed computing and com-

232 munication, where each transmitter broadcasts a signal
 233 to every receiver. As in Lolla et al (2014), the start
 234 points here are assumed to be the transmitters, the au-
 235 tonomous vehicles the “mechanical” transmission agents
 236 and the end points the locations of the receivers, i.e. where
 237 vehicles from different start points finally meet and ex-
 238 change information, for example acoustically underwa-
 239 ter. In order for the signals to be transmitted to the
 240 receivers in minimum time, it then suffices to compute
 241 the time-optimal trajectories of these autonomous vehi-
 242 cles, starting at each transmitter location and reaching
 243 every receiver location. We use our level set methodol-
 244 ogy to determine these trajectories, solving (6) for each
 245 start point, until either the level set front crosses all
 246 end points or an endurance limit is reached, whichever
 247 occurs first. Backtracking (8) is then performed to com-
 248 pute the time-optimal trajectories between every com-
 249 bination of start and end points.

Problem Setup. In all of the broadcast examples we il-

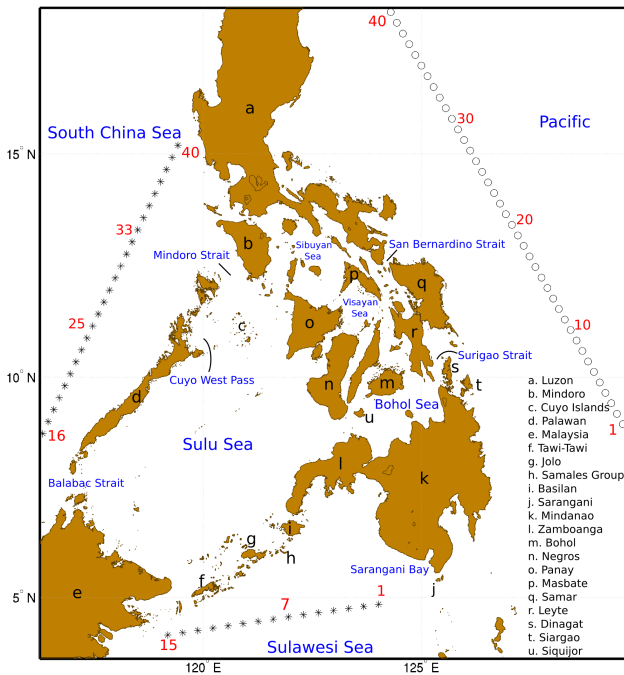


Fig. 2: All-to-all Broadcast Setup: Transmitter locations are depicted by black circles, the receiver locations by asterisks. Major islands are alphabetically indexed in black, while water bodies are indicated in blue.

251 lustrate, there are 40 transmitters (numbered 1 through
 252 40 and depicted by round markers in Fig. 2) located in
 253 the Pacific, with coordinates uniformly spaced between
 254 $8^{\circ}56' N$ $129^{\circ}36' E$ and $18^{\circ}7' N$ $124^{\circ}17' E$. The 40 re-
 255 ceivers (depicted by star markers in Fig. 2) are divided
 256

257 into two sets: one consisting of 15 points (numbered 1–
 258 15), uniformly spaced between $4^{\circ}8' N$ $119^{\circ}11' E$ and
 259 $4^{\circ}50' N$ $124^{\circ}1' E$ in the Sulawesi Sea, while the second
 260 set consists of 25 end points (numbered 16–40) in the
 261 South China Sea, uniformly spaced between $8^{\circ}44' N$
 262 $116^{\circ}20' E$ and $15^{\circ}11' N$ $119^{\circ}25' E$. In total, there are
 263 thus 1600 vehicles, grouped into swarms of 40 at each
 264 start point and with each vehicle in a swarm aiming to
 265 reach a different end point in fastest time. This com-
 266 plexity and large number of vehicles are purposely se-
 267 lected to show the scalability and robustness of the
 268 method, even for missions with many more vehicles and
 269 obstacles that are typically considered today.

270 The examples employ either typical underwater glid-
 271 ers (in §3.1.1) or faster propelled vehicles (in §3.1.2).
 272 Gliders are assumed to be capable of sustaining nominal
 273 relative speeds of up to 0.25 m/s (roughly 0.5 knots),
 274 which is the average speed of most present-day under-
 275 water gliders. On the other hand, the propelled vehi-
 276 cles are assumed to have higher relative speeds, up to
 277 1 m/s. It is additionally assumed that both sets of vehi-
 278 cles have an endurance limit of 47 days, i.e. they must
 279 reach their respective receivers within this time failing
 280 which, the corresponding data transmission is deemed
 281 infeasible (this duration of 47 days is somewhat arbi-
 282 trary, it is simply representative of common sea experi-
 283 ments). The overall goal is to predict the time-optimal
 284 trajectory between every combination of transmitters
 285 and receivers in accord with the data-driven simulated
 286 ocean flow fields and the vehicle nominal speeds, so as to
 287 achieve fastest-time all-to-all broadcast of information.
 288 The specific objectives are thus to (i) predict which of
 289 the planning missions are feasible, i.e. which of the vehi-
 290 cles successfully transmit their data within 47 days of
 291 travel, and (ii) compute and analyze the fastest-time
 292 forecast trajectories for such vehicles.

3.1.1 All-to-all Broadcasts Using Underwater Gliders.

293 *Effects of Ocean Currents on Feasible Paths and Trans-*
 294 *mission Rate.* Fig. 3a shows the time-optimal trajec-
 295 tories for the vehicles that can reach their receivers within
 296 47 days of deployment. For ease of visualization, all
 297 trajectories originating from a common transmitter are
 298 identically colored. To distinguish among transmitters,
 299 a transition of colors is employed, from red (transmit-
 300 ter 1) to green (transmitter 40), going through differ-
 301 ent shades of orange and yellow. Receivers to which
 302 at least one transmitter can successfully deliver its in-
 303 formation are shaded in black while all others are left
 304 unshaded. Vehicle trajectories are overlaid on a color
 305 plot of the magnitude of the simulated ocean currents
 306 at the end of 47 days and the corresponding velocity
 307

vectors. From this figure, it is clear that receivers 16–29 do not receive data from any of the transmitters within 47 days: in other words, these locations 16–29 in the South China Sea cannot be reached from any of the start points by vehicles that have a maximum relative speed of 0.25 m/s. Furthermore, out of an overall number of 1600 vehicles, 652 of them successfully reach their receivers, indicating a transmission rate of roughly 40%.

To illustrate the effect of currents on the minimum-time paths and on the transmission rate, we show in Fig. 3b the time-optimal trajectories between transmitters and receivers, computed ignoring ocean currents. Specifically, we set $\mathbf{V}(\mathbf{x}, t) = \mathbf{0}$ in (6) and (8). As in Fig. 3a, trajectories of only those vehicles that reach their receivers within 47 days are shown. As expected, the optimal trajectories are composed of straight line segments, i.e., leading to minimum Euclidean distance while avoiding all landforms. In this case, only 14 receivers (1–6 and 33–40) receive any data from the transmitters and only 139 of the 1600 vehicles successfully reach their receivers in 47 days. This is a prediction of a transmission rate of about 9%, which is much lower than the previous case where flow effects are taken into account. For path planning, this result highlights the importance of utilizing flow estimates when they are available and sufficiently accurate (e.g. ocean forecasts up to their predictive capability limit).

We note here that the case of zero relative speed ($F = 0$) corresponds to drifters, which are agents that have no steering or propelling mechanism of their own and are simply advected by the flow. In other words, they behave as Lagrangian particles and their positions/trajectories are governed by (6) and (8), with $F = 0$. We actually ran this case for many drifters (not shown). We found all are either advected by the Mindanao current or the Kuroshio, none of them getting close to end points.

Global Analysis of Trajectories. Time-optimal glider trajectories in the above two cases are now examined. In doing so, we explain how they are affected by ocean currents and motivate the need for such predictive path-planning for underwater missions. The islands, seas and straits referenced below are specified in Fig. 2.

Prior to performing the path planning, one could think that the fastest route to receivers in the Sulawesi Sea is through the Surigao strait and Bohol sea. However, we find that the time-optimal trajectories to all points in the Sulawesi Sea utilize the Mindanao current (south-east of Mindanao island, see Fig. 1) and, as a result, none of them go through the Bohol (Fig. 3a). Though the flow through Surigao strait into the Bohol is quite strong at the right tidal period, the largely

anticlockwise currents encountered by vehicles upon exiting the Bohol drive the vehicles northward, away from the Sulawesi. In addition, the tidal currents within the straits of the Sulu Archipelago between Mindanao and Malaysia are strong and challenging to overcome. In contrast, the Mindanao current is always favorable and all Sulawesi-bound vehicles utilize it. When flow effects are ignored (Fig. 3b), far fewer vehicles reach the Sulawesi and this highlights the importance of using the Mindanao current to minimize travel time.

Optimal trajectories from transmitters 15–40 leading to the Sulawesi converge onto a common segment from just offshore of Surigao Strait until they go around Mindanao island, after which they disperse towards their respective receiver locations (Fig. 3a). When the flow is ignored, no vehicle from these transmitters makes it to the Sulawesi within 47 days.

Trajectories to receivers 30–40 in the South China Sea pass through both the northern and southern sides of Mindoro island (Fig. 3a). The presence of green colored trajectories on both sides of the island suggests that there is considerable sensitivity of optimal trajectories to the transmitter starting locations.

The curvy nature of trajectories in the Pacific from transmitters 7–40 reflects the presence of meandering currents, jets and large-scale eddies that assist vehicles in minimizing their travel time. This can also be verified from the flow-field snapshots in Fig. 1a-d. For example, vehicles from orange start points (7–18) travelling to the Sulawesi Sea divide into three main paths. The southernmost orange paths travel first to the southeast, by coincidence right along the line of transmitters, so as to catch the Mindanao current and associated wind-driven jets: travelling along the transmitters is the roughly shortest route (orthogonal) to the Mindanao current.

Even though start points determine the optimal paths, one can see from our coloring scheme that vehicles tend to cluster into groups, travelling along favorable strong currents or away from unfavorable strong currents, even if start points are relatively far apart. This indicates that the time-optimal paths are related under certain conditions to the paths following Lagrangian Coherent Structures which are skeletons of the flow (Inanc et al, 2005; Hsieh et al, 2012; Michini et al, 2014). In the present case, this is also in part because the total length of the paths is long compared to the distance between start points. For example, trajectories from transmitters 15–40 (green and yellow) to receivers in the South China Sea converge and pass through San Bernardino strait after which they split into two groups, just north of Masbate island. However, vehicles start-

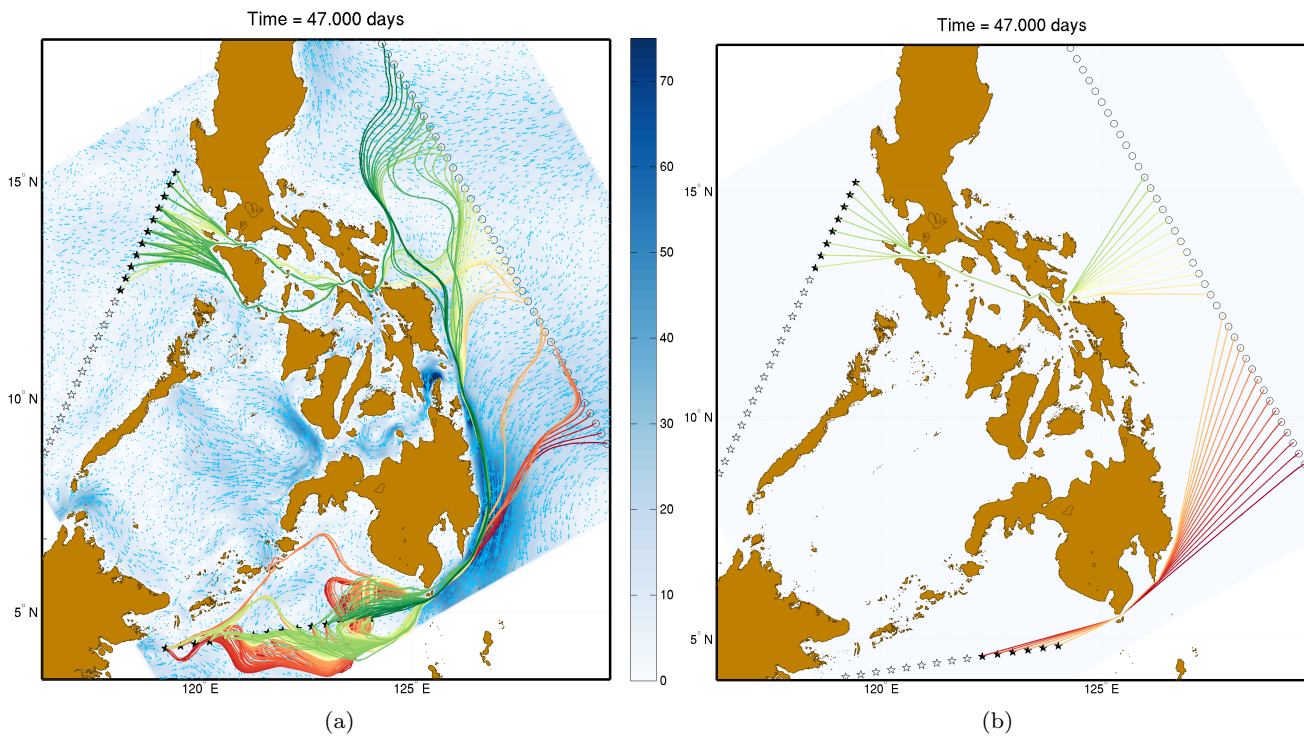


Fig. 3: Time-optimal trajectories of underwater gliders employed in the all-to-all broadcast mission, computed by (a) taking the flow-field into account and (b) ignoring the flow-field. Only trajectories of gliders that can complete their journeys within 47 days of deployment are shown.

413 ing from nearby transmitter locations can also end up
414 in different clusters, as discussed above.

415 *Local Analysis of Trajectories in the Sulawesi Sea.*
416 We now analyze the optimal glider trajectories in the
417 Sulawesi. This is because the region exhibits several
418 interesting flow features with strong tidal currents in
419 straits, highly unsteady jets and multi-scale eddies with
420 varying strengths and directions of rotation. These fea-
421 tures lead to diverse vehicle trajectories. Though the
422 trajectories enter the Sulawesi Sea from a small com-
423 mon area around Sarangani islands south of Mindanao
424 (see Fig. 4a), their final segments are starkly different.

425 Vehicles corresponding to red transmitters arrive
426 first and encounter a cyclonic (anticlockwise) current
427 in the Sarangani bay, upon entering the Sulawesi Sea
428 (see Fig. 4b). This current forces them slightly north-
429 ward, away from the line of receivers. The current then
430 turns, enabling vehicles to head back south, by riding
431 along a double-gyre flow (see Fig. 4c). As this double-
432 gyre flow is strong, most vehicles overshoot the line of
433 receivers and wait for a favorable anticyclonic (clock-
434 wise) eddy to drive them northward again (Fig. 4d,e,f).
435 This overshooting occurs once more for some of the fur-
436 ther westbound trajectories (those leading to receivers
437 11–15, see Fig. 4g,h). In all cases, as expected, the vehi-

cles minimize their travel time by utilizing various flow
438 features in the Sulawesi Sea.
439

440 Orange trajectories behave, for the most part, simi-
441 lar to their red counterparts. Though these vehicles
442 reach the Sarangani islands about 4 days after the red
443 ones (Fig. 4b), they still experience the cyclonic cur-
444 rent upon their entrance to the Sulawesi Sea. They too,
445 exhibit patterns of overshoots on their way to their re-
446 spective receivers (Fig. 4d). A particularly interesting
447 aspect of the orange trajectories is that a small subset
448 of them goes northwest right up to the Basilan island
449 south of Zamboanga peninsula (Fig. 4e) in the Sulu
450 Archipelago, then rides to the southwest, going around
451 the Samales group at right time for favorable or weaker
452 tidal currents (Fig. 4f). They then utilize a coastal jet
453 to finally reach receivers 12–15 (Fig. 4g–i).

454 It is striking to find out that vehicles originating
455 from yellow transmitters split into two groups when
456 they enter the Sulawesi Sea (Fig. 4c). The smaller group,
457 heading towards receivers 1–3, deviates northward simi-
458 lar to red and orange trajectories. Most of the yellow
459 vehicles however, travel south of the array of receivers
460 and ride a favorable jet meandering among eddies to
461 reach their respective end points (Fig. 4e–f). A small

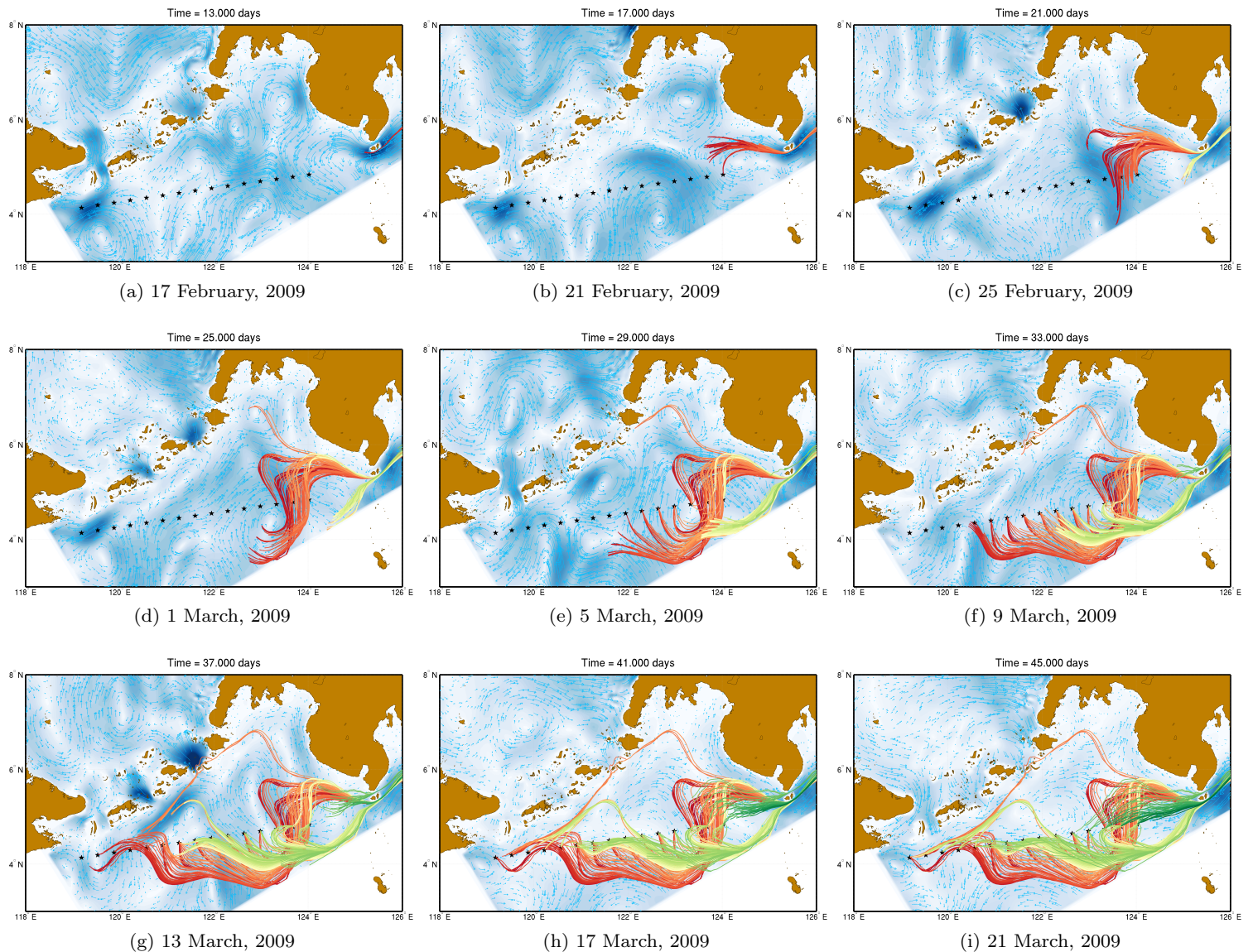


Fig. 4: Time-optimal glider trajectory segments in the Sulawesi Sea on various dates and their dependence on the local flow-field. Remarkable differences between trajectories are observed due to the variability over time.

462 subset of these vehicles experiences overshoots from the
463 line of receivers to reach end points 11–15 (Fig. 4h–i).

464 Finally, aided by the Mindanao current, vehicles cor-
465 responding to green trajectories reach the Sulawesi Sea
466 more than 20 days after the red ones (Fig. 4f). By this
467 time, the strength of the coastal current of the cyclonic
468 eddy past Sarangani Bay has ebbed (Fig. 4d) and re-
469 versed, allowing some of vehicles to travel through the
470 Sarangani strait. As a result, green trajectories that
471 reach receivers 1–5 are forced northward to a much
472 lesser extent than some of the red or orange ones (Fig. 4h–
473 i). However, none of the darker green vehicles make it
474 to end points 6–15 within 47 days.

3.1.2 All-to-all Broadcast Using High-Speed Propelled 475
Vehicles. 476

In §3.1.1, we illustrated and analyzed various prop- 477
erties of the time-optimal paths of typical underwa- 478
ter gliders for all-to-all broadcast missions. We found 479
that even upon taking the ocean flows into account, 480
only 40% of the gliders can successfully complete their 481
broadcast missions within 47 days. We now examine 482
the effect of increasing the relative speed of vehicles on 483
the time-optimal trajectories. In addition, we estimate 484
lower bounds on their endurance limit that will allow 485
all vehicles to complete their missions. 486

487 The propelled vehicles have a maximum relative speed
 488 of 1 m/s, i.e. 4 times larger than the gliders in §3.1.1.
 489 Their endurance limit is hypothetically assumed to be
 490 same as earlier, i.e. 47 days. Numerical schemes and pa-
 491 rameters used to solve (6) and (8) in this example are
 492 identical to those used in §3.1.1. The resulting time-
 493 optimal propelled vehicle trajectories are depicted in
 494 Fig. 5.

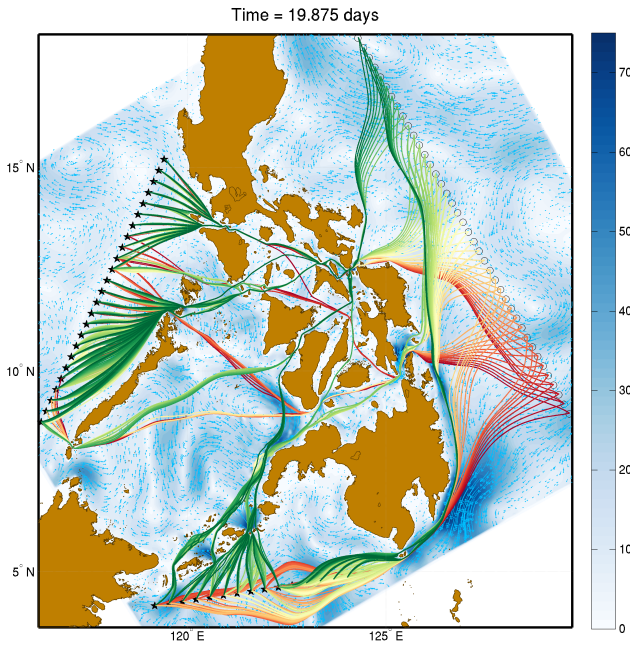


Fig. 5: Time-optimal trajectories of propelled vehicles employed in the all-to-all broadcast mission. Their higher speeds enable the mission to be completed in less than 20 days, with complete transmission.

495 *Effects of Ocean Currents on Feasible Paths and*
 496 *Transmission Rate.* From Fig. 5, we find that all of the
 497 1600 vehicles can successfully reach their receivers, result-
 498 ing in perfect transmission. In fact, all vehicles reach
 499 their respective end points in less than 20 days. There-
 500 fore, 20 days is an approximate lower limit for 1 m/s
 501 propelled vehicle endurance needed for their usage in
 502 this mission. The ability of underwater vehicles to sus-
 503 tain higher speeds usually incurs an expense of lower
 504 endurance, and our methodology reveals that if such
 505 propelled vehicles can sustain missions longer than 20
 506 days, they can be safely employed for this all-to-all in-
 507 formation broadcast.

508 Optimal trajectories of propelled vehicles (Fig. 5)
 509 are far less winding than those of gliders (Fig. 3a): due
 510 to their higher relative speed, propelled vehicles are not
 511 as affected by the ocean currents. From Fig. 3a, we find
 512 that none of the optimal trajectories of successful glid-

ers passes through the Sulu Sea. In contrast, several
 513 propelled vehicles go through the Sulu Sea on the way
 514 to their respective receivers. Among the vehicles going
 515 through the Sulu Sea, those starting from green trans-
 516 mitters go through the San Bernardino strait, while
 517 those from orange and red transmitters enter through
 518 the Surigao strait. Vehicles heading to receivers 16–31
 519 in the South China Sea cut across the Sulu Sea and
 520 enter the South China Sea, skirting the Palawan island
 521 from the north (Cuyo west pass) or the south (Balabac
 522 strait). Considering the other receivers 6–15 in the Su-
 523 lawesi Sea, from Fig. 3, we had found that green gliders
 524 could not make it there within 47 days. However, green
 525 propelled vehicles to the same receivers 6–15 ride the
 526 coastal currents west of the Zamboanga peninsula and
 527 enter the Sulawesi through the Sulu archipelago, over-
 528 coming the local tidal currents.

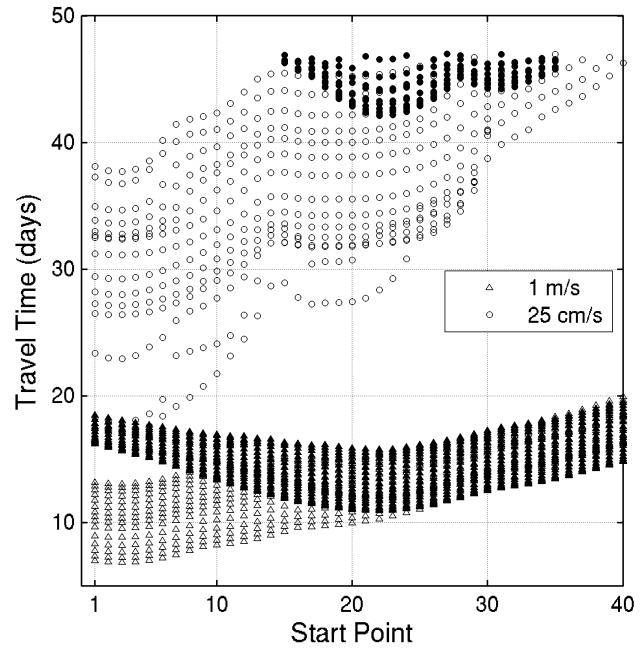


Fig. 6: Travel time of all-to-all broadcast vehicles (gliders – round markers, propelled vehicles – triangle markers) plotted against their respective start points. Shaded markers correspond to receivers in the South China Sea, unshaded ones to those in the Sulawesi Sea.

529 *3.1.3 Shortest Travel Times and Feasible Paths:*
 530 *Synthesis.*

531 To synthesize results, the computed shortest travel time
 532 (in days) of each vehicle that successfully reaches its re-
 533 ceiver is shown on a scatter plot in Fig. 6. The round
 534 markers correspond to gliders ($F = 0.25$ m/s) and
 535

the triangle markers correspond to propelled vehicles ($F = 1$ m/s). In both cases, shaded markers represent the trajectories leading to receivers 16–40 in the South China Sea, while the unshaded ones correspond to receivers 1–15 in the Sulawesi.

Starting from the southernmost transmitters 1–9, i.e. those close to Mindanao, the travel times of propelled vehicles to receivers in the Sulawesi are much less than to those in the South China Sea. As remarked earlier, this is due to the strong and favorable Mindanao current that all vehicles utilize to reach the Sulawesi Sea. The lack of shaded round markers corresponding to transmitters 1–14 (i.e. red to orange) confirm that none of these gliders reach the South China Sea. Furthermore, for these transmitters, the optimal glider travel times to the other receivers are several weeks greater than those of propelled vehicles. Considering next the line of transmitters 10–20, we find that the times of propelled vehicles to reach Sulawesi locations increase while the times to reach the South China Sea locations decrease. For these transmitters, we notice that some of the gliders start making it to the South China Sea. For transmitters 20 and higher, we find that the time taken by propelled vehicles to reach the Sulawesi steadily increases. On the other hand, the time to reach the South China Sea now also increases, after achieving a minimum for transmitter 23. This is because the vehicles pass through the San Bernardino strait, the distance to which increases for transmitters 24 and above, extending the overall travel time. For transmitters higher than 20, we find that increasingly fewer gliders make it to their designated receivers. In fact, only one glider starting from transmitter 40 is able to reach its receiver in 47 days.

3.2 Reachability of the Sulu Sea.

In underwater sensing missions such as those needed for ocean science surveys, coastal monitoring, asset inspections or naval surveillance, it is of great interest to predict which areas of the field are feasible to explore, taking into account vehicle capabilities. A common question is then: for given vehicles and ocean region, what are the locations that can and cannot be reached within a certain time limit? One estimate of such a reachable area is obtained by ignoring the ocean flows and coastlines. The reachable area is then simply a circle centered at the start point, with radius equal to the maximum straight-line distance the vehicle can travel within a given time. However, as seen from §3.1.1, ignoring the effect of ocean currents is incorrect, especially when their strength is comparable to the nominal

vehicle speed. Similarly, if there are coastlines and islands, the reachable area has to be built around them. Critically, our methodology rigorously and efficiently predicts these areas, accounting for all flow and geometry effects and for the vehicle endurance and nominal speed. This is illustrated next for the Sulu Sea.

Problem Setup. We assume that underwater gliders can be utilized up to 47 days, have a maximum relative speed of 0.25 m/s and are deployed from the same forty points in the Pacific ocean as in §3.1. To illustrate paths, the Sulu Sea region is uniformly sampled using 150 points, arranged in the form of a 15×10 rectangular array (see Fig. 7). These points are the set of end points for the underwater gliders. The goal is to predict the parts of that Sulu Sea rectangle that can be explored by gliders within 47 days, i.e. the portion of the reachable sets that overlap with the rectangle. We also illustrate this by determining which of the 150 end points can be reached by feasible paths.

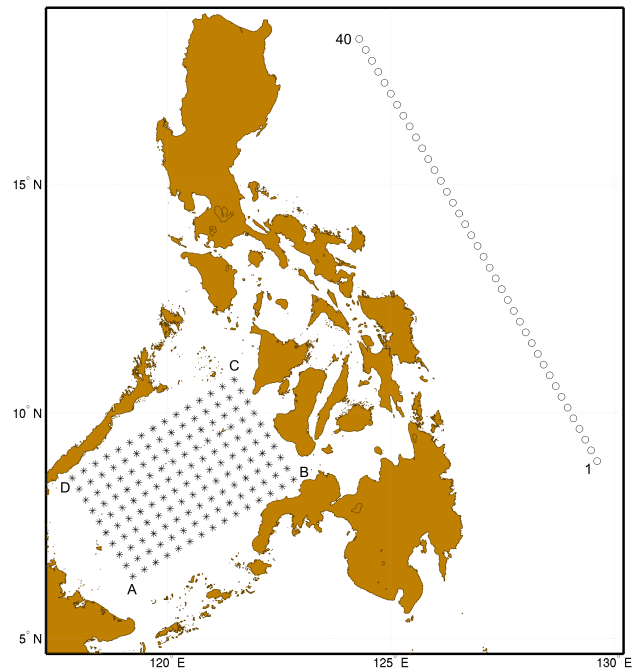


Fig. 7: Sulu Domain Setup. Forty points in the Pacific ocean are the possible start points. The rectangular area target-to-reach in the Sulu Sea has limiting vertices given by - **A**: $6^{\circ}23' N 119^{\circ}14' E$; **B**: $8^{\circ}32' N 122^{\circ}50' E$; **C**: $10^{\circ}44' N 121^{\circ}29' E$; **D**: $8^{\circ}34' N 117^{\circ}52' E$.

3.2.1 Reachable Sets.

For each of the 40 start points, the forward level set equation (6) is solved using the same numerical schemes

and parameters as those used in §3.1.1. The simulation is run up to a non-dimensional time of 376, which corresponds to the endurance limit of 47 days. The zero-level set of ϕ^o is then extracted to yield the boundary of the reachable set.

The final time reachability fronts corresponding to start points 1, 20 and 40 are shown in Fig. 8. End points that can be reached within 47 days are shaded in black, while those that cannot be reached from any start point are left unshaded (as in §3.1.1). It is clear that vehicles from start point 40, which is furthest away from the Sulu, can cover a much smaller portion of the Sulu compared to those from start points 1 and 20. Moreover, as the shape of the reachability fronts in Fig. 8 are quite different from a circle, this suggests a strong influence of islands and the ocean currents on the reachability set: in fact, the sharp angles in the front indicate that characteristic paths have merged. To further illustrate these results, the time-optimal trajectories reaching each of the shaded end points is computed by solving the backtracking equation (8). Fig. 9 depicts these optimal trajectories corresponding to all of the 40 start points. The trajectories are colored as in §3.1.1.

3.2.2 Feasible Time-Optimal Paths.

Vehicles corresponding to green trajectories utilize currents and eddies in the Pacific to reach the San Bernardino strait on their way to the Sulu Sea. This is apparent from the curvy nature of their trajectories in the Pacific. These vehicles then split into two groups, and go through either side of the Masbate and Panay islands before entering the Sulu Sea. The strong and predominantly cyclonic swirl of ocean currents encountered by vehicles that enter the Sulu from the south of Panay island forces most of them westward before they can head south toward their respective end points. Green vehicles that enter Sulu from the north of Panay island again split into multiple groups, most of which go through the Cuyo archipelago into the Sulu Sea, avoiding the islands along the way.

A small fraction of green vehicles enters the Sulu, somewhat counter-intuitively, through the Bohol sea. These vehicles utilize the strong tidal currents near the Surigao to enter the Bohol sea. They ride the northwestern coastal current along Negros island to reach their end points.

Similar to the latter green trajectories, yellow vehicles enter the Sulu through the Surigao strait and the Bohol sea. The proximity of the yellow starting points to the Surigao strait allows these vehicles to enter Bohol several days earlier than any of the green ones. Until the yellow vehicles exit the Bohol sea, their trajectories are

closely spaced, indicating that the currents in the Bohol are quite strong and that all vehicles favorably use them. Upon exiting the Bohol sea, the vehicles disperse towards their respective end points. The northwestern coastal current along Negros and its cyclonic extension in the Sulu assists vehicles that are headed towards northern end points and hinders those whose end points are located in the central and southern Sulu. For example, after a time of approximately 30 days, a subset of the yellow tracks shoots north-westward along Negros, towards Palawan Island and away from the southern end points, only to head south later.

The red tracks reach the Sulu in one of two ways: a fraction of them enters through the Bohol Sea and the others utilize the Mindanao current, go around Mindanao, and enter through the gap between Zamboanga peninsula and Basilan island. These southern tracks are also quite closely spaced until they pass Basilan island. It is interesting to note that none of these southern trajectories are able to reach the northern end points in the Sulu within 47 days. They only reach end points in the southern Sulu. Red tracks that pass through the Surigao strait and the Bohol Sea exhibit a behavior similar to the yellow tracks discussed above.

A close examination of the region just west of Basilan island reveals a sharp northwest turn and sharp smaller-scale meanders for the red and orange trajectories. This is because of the strong and sporadic, mostly tidally-driven, southeast-bound currents between Basilan and Jolo islands. When these intermittent currents appear, they force the red and orange trajectories marginally off-track, causing the local zig-zag pattern in the trajectories.

3.3 Fastest-Time Interception.

A common issue in autonomous operation is to recuperate the vehicles at the end of their mission as efficiently as possible. A directly related challenge is to predict the headings history that will lead to the fastest-time intercept between two ocean platforms. With these motivations, we now illustrate the application of our new methodology to determine fastest-time interception strategies for deployed underwater vehicles. Given a choice of multiple pick-up channels such as ships (mobile) and moorings (stationary), we are interested in navigating the underwater vessels so that they can be safely picked-up by any of the available channels in the shortest time. A key difference between this analysis and the ones previously considered is that the end points of the vehicles are not fixed a priori, but need to be chosen based on which pick up channel can be reached faster. Another key difference is that some of

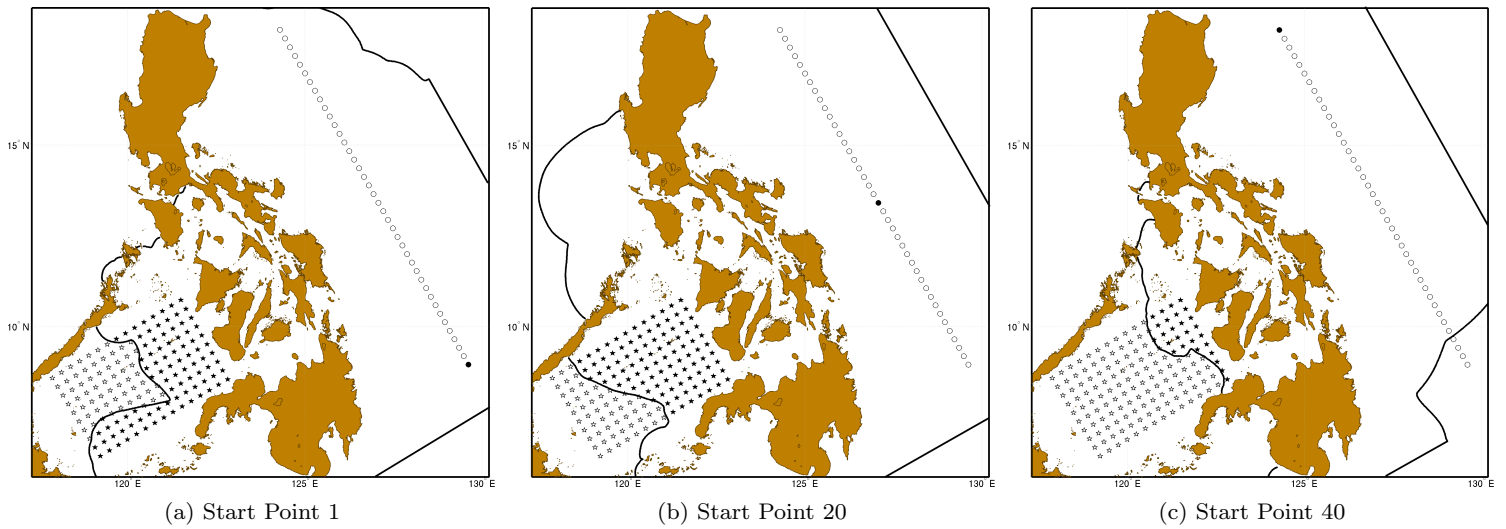


Fig. 8: Final-time reachability fronts of gliders released from different points in the Pacific ocean. The reachability fronts separate the Sulu sea into two regions, one that can be reached by gliders inside 47 days (shaded star markers) and one that cannot (unshaded star markers).

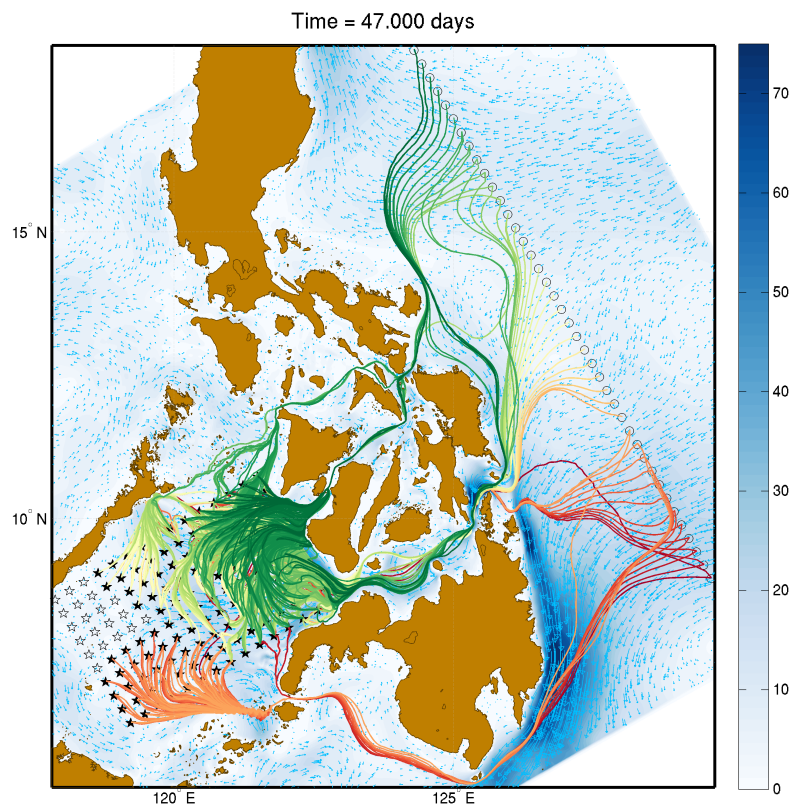


Fig. 9: Time-optimal trajectories of gliders released in the Pacific ocean as on Fig. 8 and leading to end points in the Sulu Sea. Only trajectories of gliders that can complete their journeys within 47 days of deployment are shown.

711 the end points are mobile, i.e. the underway vessels.

712

713 *Problem Setup.* Twelve underwater gliders, numbered
714 serially (see Fig. 10), are initially spread out in varied

715 internal seas of the Philippines Archipelago. The first
716 seven gliders are located in the Sibuyan sea, the eighth
717 in the Visayan sea and the others in the Bohol sea. The
718 gliders may be picked up by any of three channels: two

715

716

717

718

719 moving ships, one in the Pacific ocean and one in the
 720 South China Sea; and one mooring stationed in the Sulu
 721 Sea at coordinates $8^{\circ}12' N$ $120^{\circ}39' E$. The Pacific ship
 722 is assumed to continuously patrol between coordinates
 723 $9^{\circ}46' N$ $128^{\circ}50' E$ and $16^{\circ}49' N$ $124^{\circ}45' E$, while the
 724 South China Sea ship moves back and forth between
 725 $9^{\circ}48' N$ $118^{\circ}4' E$ and $15^{\circ}22' N$ $119^{\circ}26' E$. Both ships are
 726 initially located at their lowest respective longitudes,
 727 and are assumed to sail at absolute nominal speeds of
 728 5 m/s (roughly 10 knots). As the speeds of the ocean
 729 currents are much smaller than the nominal speeds of
 730 both ships, we neglect the effect of currents on the ships'
 731 motion (even though it can be accounted for if needed).

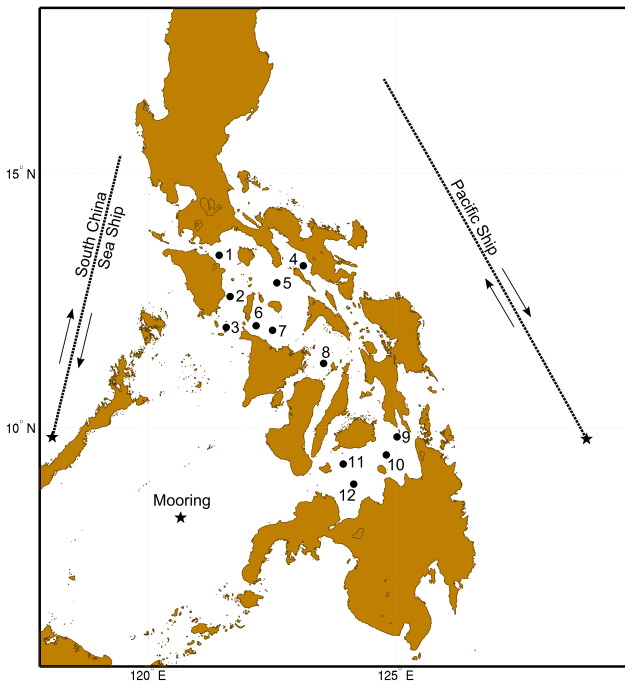


Fig. 10: Schematic of Fastest-Time Pickup: twelve gliders are to be picked-up in fastest-time by either two underway ships or a fixed station (e.g. mooring).

732
 733 In order to determine the headings for the fastest
 734 pick-up, we solve (6) starting from the initial positions
 735 of each glider. During the course of the evolution of the
 736 corresponding reachability fronts, we keep track of the
 737 underway positions of both ships. The evolution of the
 738 reachability fronts is terminated when they encounter
 739 either of the ships, or the stationary mooring. Back-
 740 tracking (8) is then performed to compute the optimal
 741 trajectories.

742 *Interception Locations and Time-Optimal Paths.* The
 743 end locations and platforms, and the corresponding tra-
 744 jectories, that correspond to the time-optimal for pick-

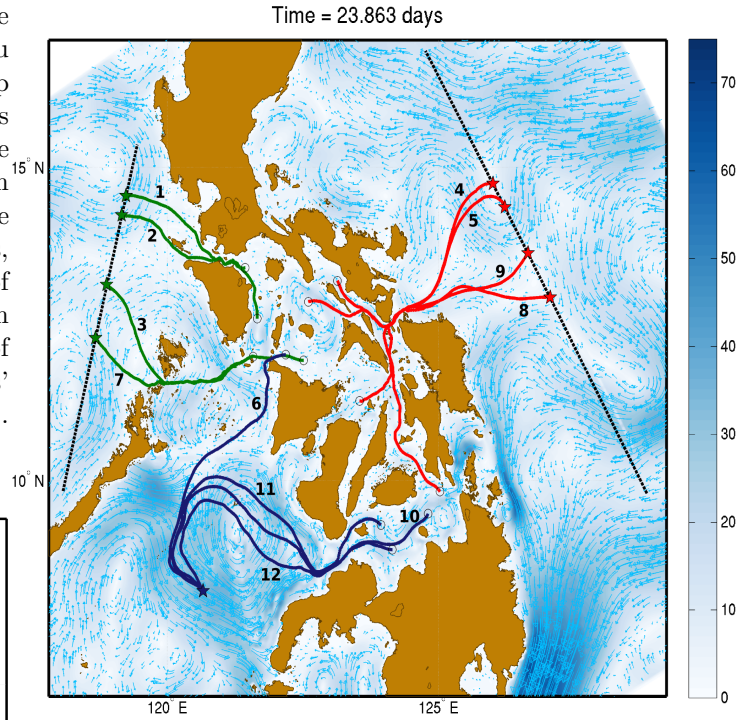


Fig. 11: Fastest-time pickup trajectories of gliders. In addition to the optimal trajectory, the pickup platform and location are computed by the methodology.

745 up are plotted in Fig. 11. Trajectories of gliders col-
 746 lected by the South China Sea ship, Pacific ship and
 747 mooring are colored in green, red and blue, respective-
 748 ly. By inspecting these results, several interesting obser-
 749 vations can be made. We see that the gliders 1, 2, 3 and 7
 750 are picked up by the South China Sea ship, while glid-
 751 ers 6, 10, 11 and 12 reach the mooring faster than they
 752 reach either of the ships. The rest of the gliders are in-
 753 tercepted by the Pacific ship. Gliders 1–3 are closest to
 754 the South China Sea and it is reasonable that they head
 755 towards the corresponding ship. Interestingly, glider 6,
 756 despite being closer to South China Sea than glider 7,
 757 is picked up by the mooring. Gliders 10, 11 and 12 uti-
 758 lize the currents entering the Sulu through the Bohol to
 759 minimize their travel time. The optimal glider 9 how-
 760 ever, though initially located in the Bohol Sea near the
 761 Surigao strait, takes the route to the Pacific through
 762 the San Bernardino strait. Gliders 4, 5 and 8 also pass
 763 through the San Bernardino strait and get picked up
 764 by the Pacific ship. Owing to the strong inflows into
 765 the Bohol sea through the Surigao strait, none of the
 766 gliders sail upstream through the Surigao, but instead
 767 enter the Pacific through the San Bernardino strait.

4 Conclusions.

We illustrated and analyzed the capabilities of our rigorous time-optimal path planning methodology in the Philippine Archipelago region, for a wide range of planning scenarios and vehicle types. The region was chosen because of its complex geometry and multiscale flows, providing challenging environments for the planning of autonomous underwater missions. The multiscale flows encountered by the vehicles, including variable large-scale currents, strong jets, eddies, wind-driven currents and tides, were simulated using the MSEAS data-assimilative primitive-equation ocean modeling system. Using these flows, we computed and analyzed the time-optimal paths of large swarms of gliders and propelled vehicles performing all-to-all broadcast missions through the archipelago. The effects of the multiscale flows and vehicle nominal speeds on the feasible trajectories and on the overall information transmission rates were discussed and synthesized. We also used our level set method for planning the deployment of vehicles, specifically predicting which portion of a specific region can be reached and explored within a given time. Such reachability analyses were exemplified for the Sulu Sea. We then applied our method to the recovery of vehicles and computed the vehicles headings time-history that lead to the fastest interception with either underway or fixed platforms. To do so, our schemes were extended to the case where end-points are variable with time and space, and not determined a priori. The results indicate the scalability and robustness of the rigorous methodology, even for complex missions in multiscale ocean environments with many more vehicles and obstacles that are typically employed today.

Some general conclusions can be drawn from the results obtained from the above examples. Irrespective of the location of end points, i.e. whether they are in the South China Sea, the Sulu Sea or in the Sulawesi Sea, trajectories of all the vehicles that start in the Pacific converged into a handful number of distinct segments until they cross the Archipelago. These segments include the San Bernardino strait, Surigao strait and southeast of Mindanao island. After crossing these ‘choke points’, vehicles disperse towards their respective end points, utilizing favorable currents and eddies as they are encountered. The overall behavior of time-optimal trajectories highlights the multi-scale features of the islands and ocean currents in the Philippines region. It also underlines the importance of utilizing the right ocean feature to go around the islands, the choice of which in several cases is not directly clear. In fact, since currents vary and even reverse over multiple scales, in response to tidal forcing, wind forcing and

internal variability, it would be challenging to estimate the vehicle headings that lead to the fastest arrival time without a rigorous path planning methodology. Reachability fronts also confirm this by their complex shapes and sharp angles indicative of merging characteristics. We also showed that ocean currents when properly utilized will allow more efficient missions and, in some case, will even enable the otherwise infeasible mission. These results indicates that it is now becoming critical to utilize flow predictions when they are available and sufficiently accurate, e.g. ocean forecasts up to their predictive capability limit.

Future opportunities include merging the level set path planning approach with adaptive sampling or adaptive modeling schemes (e.g., Yilmaz et al, 2006; Lermusiaux, 2007; Yilmaz et al, 2008; Paley et al, 2008; Choi and How, 2010; Lolla, 2012), so as to collect observations that best sample either ocean fields or modeled processes, respectively. This would involve coupling with data assimilation schemes (Robinson et al, 1998; Sondergaard and Lermusiaux, 2013), accounting of ocean forecast uncertainty in the planning (Lermusiaux, 2006; Lermusiaux et al, 2006, 2014). Our methodology can also be extended to new missions or to other ocean platforms. This includes planning and routing for autonomous kayaks (Xu et al, 2008) or ships (Mannarini et al, 2013). It can also be applied in other environments such as planning for aircrafts of varied size, especially if they are affected significantly by local wind conditions. For more detailed reviews of future applications and possibilities, we refer to (Lolla, 2012; Lolla et al, 2014).

Acknowledgements We acknowledge the Office of Naval Research for supporting this research under grants N00014-09-1-0676 (Science of Autonomy A-MISSION), N00014-07-1-0473 (PhilEx), N00014-12-1-0944 (ONR6.2) and N00014-13-1-0518 (Multi-DA) to the Massachusetts Institute of Technology (MIT). We are grateful to our MSEAS group at MIT for discussions. We also thank the two anonymous reviewers for their useful comments.

A Level set methodology for path-planning.

In this section, we briefly review the methodology and algorithm for time-optimal path planning used in this paper. The method has its roots in (Lolla et al, 2012; Lolla, 2012). A formal proof and detailed algorithm are provided in the companion paper (Lolla et al, 2014). Let $\Omega \subseteq \mathbb{R}^2$ be an open set and let $F > 0$. Suppose a vehicle (denoted by P) moves in Ω under the influence of a bounded, Lipschitz continuous dynamic flow-field $\mathbf{V}(\mathbf{x}, t) : \Omega \times [0, \infty) \rightarrow \mathbb{R}^2$. Let its start point and end point be \mathbf{y}_s and \mathbf{y}_f respectively, with $\mathbf{y}_s, \mathbf{y}_f \in \Omega$. The vehicle’s trajectory, denoted by $\mathbf{X}_P(\mathbf{y}_s, t)$ follows the kinematic relation

$$\frac{d\mathbf{X}_P}{dt} = F_P(t) \hat{\mathbf{h}}(t) + \mathbf{V}(\mathbf{X}_P(\mathbf{y}_s, t)), \quad t > 0, \quad (1)$$

where $F_P(t) \in [0, F]$ is the nominal speed of the vehicle relative to the flow and $\hat{\mathbf{h}}(t)$ is the unit vector in the steering (heading) direction. The limiting conditions on $\mathbf{X}_P(\mathbf{y}_s, t)$ are

$$\mathbf{X}_P(\mathbf{y}_s, 0) = \mathbf{y}_s, \quad \mathbf{X}_P(\mathbf{y}_s, \tilde{T}(\mathbf{y}_f)) = \mathbf{y}_f, \quad (2)$$

where $\tilde{T}(\mathbf{y}) : \Omega \rightarrow \mathbb{R}$ is the first ‘arrival time’ at point \mathbf{y} , i.e., the first time P reaches \mathbf{y} . In this paper, it is assumed that $\mathbf{V}(\mathbf{x}, t)$ is completely known. This may correspond to the mean or the mode of the forecast flow-field given by an ocean modeling system (Lermusiaux et al, 2006; Haley and Lermusiaux, 2010; Ueckermann et al, 2013). Furthermore, a kinematic model (1) for the interaction between the flow and the vehicle is assumed to be adequate. This assumption is reasonable for sufficiently long distance underwater path planning. In addition, the notation $|\bullet|$ denotes the l-2 norm of \bullet . $F_P(t)$ and $\hat{\mathbf{h}}(t)$ together constitute the (isotropic) controls of the vehicle. For a general end point $\mathbf{y} \in \Omega$, let $F_P^o(t)$ and $\hat{\mathbf{h}}^o(t)$ be the corresponding optimal controls, i.e., controls that minimize $\tilde{T}(\mathbf{y})$ subject to the constraints (1)–(2). Let this minimum arrival time be denoted by $T^o(\mathbf{y})$, and the resultant optimal trajectory be $\mathbf{X}_P^o(\mathbf{y}_s, t)$. For the specific end point $\mathbf{y}_f \in \Omega$, the superscript ‘o’ on quantities specific to the optimal trajectory is replaced by ‘*’.

A.1 Methodology.

The path planning methodology described in (Lolla et al, 2012, 2014) involves computing the *reachable set* from a given starting point. The reachable set at any time $t \geq 0$, denoted by $\mathcal{R}(\mathbf{y}_s, t)$, is defined as the set of all points $\mathbf{y} \in \Omega$ for which there exist controls $F_P(\tau)$ and $\hat{\mathbf{h}}(\tau)$ for $0 \leq \tau \leq t$ and a resultant trajectory $\tilde{\mathbf{X}}_P(\mathbf{y}_s, \tau)$ satisfying (1) such that $\tilde{\mathbf{X}}_P(\mathbf{y}_s, t) = \mathbf{y}$. Hence, $\mathcal{R}(\mathbf{y}_s, t)$ includes only those points which can be visited by the vehicle at time t . The boundary of the reachable set is called the *reachability front*, and is denoted by $\partial\mathcal{R}(\mathbf{y}_s, t)$. As a result, for any $\mathbf{y} \in \Omega$, $T^o(\mathbf{y})$ is the first time the reachability front $\partial\mathcal{R}(\mathbf{y}_s, t)$ reaches \mathbf{y} .

We showed in (Lolla et al, 2014) that the reachable set $\mathcal{R}(\mathbf{y}_s, t)$ is related to $\phi^o : \Omega \times [0, \infty) \rightarrow \mathbb{R}$, the viscosity solution of the Hamilton–Jacobi equation. Specifically, at any given time $t \geq 0$,

$$\mathbf{x} \in \mathcal{R}(\mathbf{y}_s, t) \iff \phi^o(\mathbf{x}, t) \leq 0. \quad (3)$$

Eq. (3) implies that the zero level set of ϕ^o coincides with the reachability front $\partial\mathcal{R}(\mathbf{y}_s, t)$ for any $t \geq 0$. This relationship between reachability and level sets of ϕ^o enables an implicit computation of $\mathcal{R}(\mathbf{y}_s, t)$ by numerically solving (6)–(7).

In addition to the optimal arrival time $T^o(\mathbf{y})$, ϕ^o also yields the optimal controls $F_P^o(t)$, $\hat{\mathbf{h}}^o(t)$ and trajectory $\mathbf{X}_P^o(\mathbf{y}_s, t)$ leading to \mathbf{y} . We showed in (Lolla et al, 2014) that $\phi^o(\mathbf{X}_P^o(\mathbf{y}_s, t), t) = 0$ for all $0 \leq t \leq T^o(\mathbf{y})$, i.e., vehicles on optimal trajectories always remain on the zero level set of ϕ^o . The optimal controls, for $0 < t < T^o(\mathbf{y})$ are

$$F_P^o(t) = F, \quad \hat{\mathbf{h}}^o(t) = \frac{\nabla\phi^o(\mathbf{X}_P^o(\mathbf{y}_s, t), t)}{|\nabla\phi^o(\mathbf{X}_P^o(\mathbf{y}_s, t), t)|}, \quad (4)$$

whenever all the terms are well-defined. Equivalently, if ϕ^o is differentiable at $(\mathbf{X}_P^o(\mathbf{y}_s, t), t)$ for some $t \in (0, T^o(\mathbf{y}))$, then,

$$\frac{d\mathbf{X}_P^o}{dt} = F \frac{\nabla\phi^o(\mathbf{X}_P^o(\mathbf{y}_s, t), t)}{|\nabla\phi^o(\mathbf{X}_P^o(\mathbf{y}_s, t), t)|} + \mathbf{V}(\mathbf{X}_P^o(\mathbf{y}_s, t), t), \quad (5)$$

i.e., the optimal steering direction is normal to level sets of ϕ^o , and the optimal relative speed of the vehicle is F .

A.2 Algorithm.

The above discussion leads to an algorithm for minimum time path planning, given: $\mathbf{y}_s, \mathbf{y}_f, F, \mathbf{V}(\mathbf{x}, t)$. The algorithm comprises of the following two steps.

1. **Forward Propagation.** First, the reachability front $\partial\mathcal{R}(\mathbf{y}_s, t)$ is evolved by solving the Hamilton–Jacobi equation (6) forward in time, with initial conditions (7). The front is evolved until it reaches \mathbf{y}_f .

$$\frac{\partial\phi^o}{\partial t} + F|\nabla\phi^o| + \mathbf{V}(\mathbf{x}, t) \cdot \nabla\phi^o = 0 \quad \text{in } \Omega \times (0, \infty), \quad (6)$$

with initial conditions

$$\phi^o(\mathbf{x}, 0) = |\mathbf{x} - \mathbf{y}_s|, \quad \mathbf{x} \in \Omega. \quad (7)$$

2. **Backward Vehicle Tracking.** After the front reaches \mathbf{y}_f , the optimal vehicle trajectory $\mathbf{X}_P^*(\mathbf{y}_s, t)$ and controls are computed by solving (5) backward in time, starting from \mathbf{y}_f at time $T^*(\mathbf{y}_f) = T^o(\mathbf{y}_f)$, i.e.,

$$\frac{d\mathbf{X}_P^*(\mathbf{y}_s, t)}{dt} = -F \frac{\nabla\phi^o(\mathbf{X}_P^*(\mathbf{y}_s, t))}{|\nabla\phi^o(\mathbf{X}_P^*(\mathbf{y}_s, t))|} - \mathbf{V}(\mathbf{X}_P^*(\mathbf{y}_s, t)), \quad (8)$$

with $\mathbf{X}_P^*(\mathbf{y}_s, T^*(\mathbf{y}_f)) = \mathbf{y}_f$.

The backtracking step is necessary in this algorithm since the initial heading direction, $\hat{\mathbf{h}}^o(0)$ is not known a priori. In (Lolla et al, 2014, 2012), a level set method is used to solve the Hamilton–Jacobi equation (6). As a result, efficient schemes such as the narrow-band method (Adalsteinsson and Sethian, 1995) can be employed in the numerical scheme. Moreover, level set methods are well-known to offer substantial advantages over front tracking or other particle based approaches (Sethian, 1999; Osher and Fedkiw, 2003). A thorough introduction to level set methods may be found in (Lolla, 2012). Numerical schemes used to solve (6)–(8) are outlined in (Lolla et al, 2014).

References

- Adalsteinsson D, Sethian JA (1995) A fast level set method for propagating interfaces. *Journal of Computational Physics* 118(2):269–277
- Agarwal A, Lermusiaux PFJ (2011) Statistical field estimation for complex coastal regions and archipelagos. *Ocean Modelling* 40(2):164–189, DOI doi:10.1016/j.ocemod.2011.08.001
- Beşiktepe ŞT, Lermusiaux PFJ, Robinson AR (2003) Coupled physical and biogeochemical data-driven simulations of Massachusetts Bay in late summer: real-time and postcruise data assimilation. *Journal of Marine Systems* 40-41:171–212
- Bleck R (2002) An oceanic general circulation model framed in hybrid isopycnic-cartesian coordinates. *Ocean Modelling* 4(1):55–88
- Choi HL, How JP (2010) Continuous trajectory planning of mobile sensors for informative forecasting. *Automatica* 46(8):1266–1275
- Colin MEGD, Duda TF, te Raa LA, van Zon T, Haley PJ, Lermusiaux PFJ, Leslie WG, Mirabito C, Lam FPA, Newhall AE, Lin YT, Lynch JF (2013) Time-evolving acoustic propagation modeling in a complex ocean environment. In: *OCEANS - Bergen, 2013 MTS/IEEE*, pp 1–9, DOI 10.1109/OCEANS-Bergen.2013.6608051

- Cossarini G, Lermusiaux PFJ, Solidoro C (2009) The lagoon of venice ecosystem: Seasonal dynamics and environmental guidance with uncertainty analyses and error subspace data assimilation. *Journal of Geophysical Research* 114:C0626
- Egbert GD, Erofeeva SY (2002) Efficient inverse modeling of barotropic ocean tides. *Journal of Atmospheric and Oceanic Technology* 19(2):183–204
- Gangopadhyay A, Lermusiaux PFJ, Rosenfeld L, Robinson AR, Calado L, Kim HS, Leslie WG, Haley PJ Jr (2011) The California Current System: A multiscale overview and the development of a feature-oriented regional modeling system (FORMS). *Dynamics of Atmospheres and Oceans* 52(1-2):131–169, DOI <http://dx.doi.org/10.1016/j.dynatmoce.2011.04.003>, special issue of *Dynamics of Atmospheres and Oceans* in honor of Prof. A.R.Robinson
- Gordon AL, Villanoy CL (2011) *Oceanography*. Special issue on the Philippine Straits Dynamics Experiment, vol 24. The Oceanography Society
- Gordon AL, Sprintall J, Ffield A (2011) Regional oceanography of the Philippine Archipelago. *Oceanography* 24(1):15–27
- Haley PJ Jr, Lermusiaux PFJ (2010) Multiscale two-way embedding schemes for free-surface primitive equations in the multidisciplinary simulation, estimation and assimilation system. *Ocean Dynamics* 60(6):1497–1537, DOI 10.1007/s10236-010-0349-4
- Haley PJ Jr, Lermusiaux PFJ, Robinson AR, Leslie WG, Logutov O, Cossarini G, Liang XS, Moreno P, Ramp SR, Doyle JD, Bellingham J, Chavez F, Johnston S (2009) Forecasting and reanalysis in the Monterey Bay/California Current region for the Autonomous Ocean Sampling Network-II experiment. *Deep Sea Research II* 56(3-5):127–148, DOI doi:10.1016/j.dsr2.2008.08.010
- Haley PJ Jr, Agarwal A, Lermusiaux PFJ (2014) Optimizing velocities and transports for complex coastal regions and archipelagos. *Ocean Modelling* Submitted
- Hodur RM (1997) The naval research laboratory's coupled ocean/atmosphere mesoscale prediction system (COAMPS). *Monthly Weather Review* 125(7):1414–1430
- Hsieh MA, Forgoston E, Mather TW, Schwartz IB (2012) Robotic manifold tracking of coherent structures in flows. In: *Robotics and Automation (ICRA)*, 2012 IEEE International Conference on, pp 4242–4247, DOI 10.1109/ICRA.2012.6224769
- Hurlburt HE, Metzger EJ, Sprintall J, Riedlinger SN, Arnone RA, Shinoda T, Xu X (2011) Circulation in the Philippine Archipelago simulated by 1/12° and 1/25° global HYCOM and EAS NCOM. *Oceanography* 24(1):28–47
- Inanc T, Shadden SC, Marsden JE (2005) Optimal trajectory generation in ocean flows. In: *American Control Conference*, 2005. Proceedings of the 2005, pp 674–679, DOI 10.1109/ACC.2005.1470035
- Leben RR, Born GH, Engebretth BR (2002) Operational altimeter data processing for mesoscale monitoring. *Marine Geodesy* 25(1-2):3–18
- Lermusiaux PFJ (2006) Uncertainty estimation and prediction for interdisciplinary ocean dynamics. *Journal of Computational Physics* 217:176–199
- Lermusiaux PFJ (2007) Adaptive modeling, adaptive data assimilation and adaptive sampling. *Physica D Nonlinear Phenomena* 230:172–196
- Lermusiaux PFJ, Chiu CS, Gawarkiewicz GG, Abbot P, Robinson AR, Miller RN, Haley PJ, Leslie WG, Majumdar SJ, Pang A, Lekien F (2006) Quantifying uncertainties in ocean predictions. *Oceanography* 19(1):90–103
- Lermusiaux PFJ, Haley PJ Jr, Yilmaz NK (2007) Environmental prediction, path planning and adaptive sampling-sensing and modeling for efficient ocean monitoring, management and pollution control. *Sea Technology* 48(9):35–38
- Lermusiaux PFJ, Haley PJ, Leslie WG, Agarwal A, Logutov O, Burton L (2011) Multiscale physical and biological dynamics in the philippines archipelago: Predictions and processes. *Oceanography* 24(1):70–89, DOI doi:10.5670/oceanog.2011.05
- Lermusiaux PFJ, Lolla T, Haley PJ Jr, Yigit K, Ueckermann MP, Sondergaard T, Leslie WG (2014) *Science of Autonomy: Time-Optimal Path Planning and Adaptive Sampling for Swarms of Ocean Vehicles*. Chapter 11, Springer Handbook of Ocean Engineering: Autonomous Ocean Vehicles, Subsystems and Control, Tom Curtin (Ed.), in press.
- Leslie WG, Robinson AR, Haley PJ, Logutov O, Moreno P, Lermusiaux PFJ, Coehlo E (2008) Verification and training of real-time forecasting of multi-scale ocean dynamics for maritime rapid environmental assessment. *Journal of Marine Systems* 69(1-2):3–16
- Logutov OG, Lermusiaux PFJ (2008) Inverse barotropic tidal estimation for regional ocean applications. *Ocean Modelling* 25(1-2):17–34
- Lolla T (2012) Path planning in time dependent flows using level set methods. Master's thesis, Department of Mechanical Engineering, Massachusetts Institute of Technology
- Lolla T, Ueckermann MP, Yigit K, Haley PJ, Lermusiaux PFJ (2012) Path planning in time dependent flow fields using level set methods. In: *Proceedings of IEEE International Conference on Robotics and Automation*, pp 166–173
- Lolla T, Lermusiaux PFJ, Ueckermann MP, Haley PJ Jr (2014) Time-optimal path planning in dynamic flows using level set equations: Theory and schemes. *Ocean Dynamics* Submitted
- Mannarini G, Coppini G, Oddo P, Pinardi N (2013) A prototype of ship routing decision support system for an operational oceanographic service. *TransNav, the International Journal on Marine Navigation and Safety of Sea Transportation* 7(1):53–59, DOI 10.12716/1001.07.01.06
- Michini M, Hsieh MA, Forgoston E, Schwartz IB (2014) Robotic tracking of coherent structures in flows. *IEEE Transactions on Robotics* 30(3):593–603, DOI 10.1109/TRO.2013.2295655
- MSEAS Group (2010) *Multidisciplinary Simulation, Estimation, and Assimilation Systems* (<http://mseas.mit.edu/>, <http://mseas.mit.edu/codes/>) Manual. MSEAS Report 6, MIT, Cambridge, MA, USA
- Onken R, Álvarez A, Fernández V, Vizoso G, Basterretxea G, Tintoré J, Haley P Jr, Nacini E (2008) A forecast experiment in the Balearic Sea. *Journal of Marine Systems* 71(1-2):79–98
- Osher S, Fedkiw R (2003) *Level Set Methods and Dynamic Implicit Surfaces*. Springer Verlag
- Paley DA, Zhang F, Leonard NE (2008) Cooperative control for ocean sampling: The glider coordinated control system. *IEEE Transactions on Control Systems Technology* 16(4):735–744
- Qu T, Lukas R (2003) The Bifurcation of the North Equatorial Current in the Pacific. *Journal of Physical Oceanography* 33(1):5–18
- Ramp SR, Lermusiaux PFJ, Shulman I, Chao Y, Wolf RE, Bahr FL (2011) Oceanographic and atmospheric conditions on the continental shelf north of the Monterey Bay during August 2006. *Dynamics of Atmospheres and Oceans* 52(1-

- 2):192–223
- Robinson AR, Lermusiaux PFJ, Sloan III NQ (1998) Data Assimilation. *The Sea: The Global Coastal Ocean I*, K. H. Brink and A. R. Robinson (Eds.), Volume 10, John Wiley and Sons, New York, NY, 541-594
- Sethian JA (1999) *Level Set Methods and Fast Marching Methods: Evolving Interfaces in Computational Geometry, Fluid Mechanics, Computer Vision, and Materials Science*. Cambridge University Press: Cambridge, U.K.
- Sondergaard T, Lermusiaux PFJ (2013) Data assimilation with Gaussian Mixture Models using the dynamically orthogonal field equations. Part I: Theory and Scheme. *Monthly Weather Review* 141(6):1737–1760
- Uecker mann MP, Lermusiaux PFJ, Sapsis TP (2013) Numerical schemes for dynamically orthogonal equations of stochastic fluid and ocean flows. *Journal of Computational Physics* 233(0):272 – 294
- Xu J, Lermusiaux PFJ, Haley PJ, Leslie WG, Logoutov OG (2008) Spatial and temporal variations in acoustic propagation during the PLUSNet07 exercise in dabob bay. *Proceedings of Meetings on Acoustics (POMA)*, 155th Meeting Acoustical Society of America 4:070,001
- Yilmaz NK, Evangelinos C, Patrikalakis NM, Lermusiaux PFJ, Haley PJ, Leslie WG, Robinson AR, Wang D, Schmidt H (2006) Path planning methods for adaptive sampling of environmental and acoustical ocean fields. In: *OCEANS 2006*, pp 1–6, DOI 10.1109/OCEANS.2006.306841
- Yilmaz NK, Evangelinos C, Lermusiaux PFJ, Patrikalakis NM (2008) Path planning of autonomous underwater vehicles for adaptive sampling using mixed integer linear programming. *Oceanic Engineering, IEEE Journal of* 33(4):522–537, DOI 10.1109/JOE.2008.2002105